

Stability of Equatorial Modes in a Simplified Coupled Ocean–Atmosphere Model

CHUNZAI WANG AND ROBERT H. WEISBERG

Department of Marine Science, University of South Florida, St. Petersburg, Florida

(Manuscript received 19 October 1994, in final form 17 June 1996)

ABSTRACT

The stability, periodicity, and horizontal structure of equatorial modes in a coupled ocean–atmosphere model, simplified by the assumption that zonal wind stress anomalies are proportional to sea surface temperature anomalies lagged by a zonal phase difference, are examined analytically in an unbounded basin. The gravest coupled Rossby and Kelvin modes coexist with additional westward and eastward slow modes whose phase speeds are smaller than the former. Two of these four modes, one propagating westward and the other eastward, are destabilized in each case depending upon the model parameters. For some particular parameter choices, coupled Rossby and Kelvin modes merge with westward and eastward slow modes, respectively. For other parameters, however, they separate and remain distinct from the slow modes. For all of these modes the primary modifications by coupling relative to uncoupled oceanic equatorial waves are a decrease in phase speed and an increase in meridional scale.

Among the model parameter effects, those of the zonal phase lag between the wind stress and SST anomalies and the coefficients of thermal and mechanical damping are the most interesting. Positive and negative phase lags represent the wind stress anomalies located to the west and east of the SST anomalies, respectively. The frequency of all modes is symmetric about zero phase lag, whereas the growth rate is antisymmetric about zero phase lag relative to the uncoupled damping rate. Wind stress anomalies to the west of SST anomalies favor slow mode growth and coupled Rossby and Kelvin mode decay. Dissipation for the slow modes and the coupled Rossby and Kelvin modes is controlled differently. For the slow modes the dissipation is mainly thermal, whereas for coupled Rossby and Kelvin modes the dissipation is mainly mechanical.

1. Introduction

Starting with Bjerknes's (1969) identification of unstable interactions between the tropical Pacific Ocean and the atmosphere as a possible cause of the El Niño/Southern Oscillation, oceanographers and meteorologists have focused increasingly on the coupled ocean–atmosphere system in ENSO studies. There are two ways to quantify Bjerknes's ideas: one is by using stability analyses to establish the properties of unstable modes; another is by using coupled ocean–atmosphere models marching forward in time to simulate the development of unstable modes. Many coupled ocean–atmosphere models have been explored, beginning with the conceptual model of McCreary (1983); the development of the coupling physics by Philander et al. (1984); and the subsequent applications of linear perturbation models, models linearized about different background states, and general circulation models. Within these models, the delayed oscillator (e.g., Suarez and Schopf 1988; Battisti and Hirst 1989) and the slow mode (e.g., Hirst 1988; Neelin 1991; Wang

and Weisberg 1994a) have been developed as interpretive mechanisms. The delayed oscillator depends upon uncoupled mode reflections in a bounded basin, while the slow mode may occur in an unbounded basin. Thus, analysis of stability and horizontal structure for equatorial wave modes of an unbounded basin may lead to an improved understanding of the nature of the coupled ocean–atmosphere system.

Battisti and Hirst (1989) showed that a version of the Suarez and Schopf (1988) analog delayed oscillator model could account for the model oscillations of Zebiak and Cane (1987). The analog model is represented by an ordinary differential delay equation with positive and negative feedbacks. The positive feedback is the sum of all local coupling processes, whereas the delayed negative feedback results from Kelvin modes generated at the western boundary as reflected Rossby modes. This paradigm, therefore, depends upon the relative strengths of the local positive feedback and the delayed negative feedback, which may be affected by the stability properties of the Rossby and Kelvin modes. For example, damping of these modes reduces the delayed feedback necessary to change the sign of the instability in the eastern side of ocean basin.

Hirst (1986) used numerical methods to explore the effects of four different ocean thermodynamics parameterizations on coupled modes. With sea surface tem-

Corresponding author address: Dr. Robert H. Weisberg, Dept. of Marine Science, University of South Florida, 140 Seventh Avenue South, St. Petersburg, FL 33701-5016.

perature proportional to the thermocline thickness anomaly, the oceanic Kelvin wave is destabilized (also see Lau 1981). With the rate of change of SST proportional to zonal advection and thermal damping, the gravest oceanic Rossby wave is destabilized. By considering thermocline thickness and thermal damping, with or without advection, a slowly propagating unstable mode occurs.

Relative to the delayed oscillator and slow mode mechanisms, ENSO appears to be more complicated than any one model might suggest. Both observations and models show that the meridional scale of the coupled ocean–atmosphere system is larger than an oceanic equatorial Rossby radius of deformation (e.g., Chao and Philander 1993; Latif and Barnett 1995), and ENSO events have been characterized by eastward or westward propagating or stationary disturbances. For example, the relatively simple models of Philander et al. (1984), Anderson and McCreary (1985), Hirst (1988), and Wang and Weisberg (1994a) show eastward propagation in contrast to those of Rennick (1983) and Gill (1985), which show westward propagation, and those of Zebiak and Cane (1987) and Battisti (1988), which show in-phase growth over the eastern equatorial Pacific.

Jin and Neelin (1993a,b) and Neelin and Jin (1993) attempt to consolidate such seemingly contradictory works through studies of how relatively simple models may be related in parameter space. Using an equatorial narrow band coupling approximation in the SST equation, they argued that the unstable ocean dynamics mode of Cane et al. (1990) and the unstable SST mode of Neelin (1991) represent a fast-SST limit and a fast-wave limit, respectively. In the fast-SST limit, SST adjusts more rapidly than the ocean dynamics, so SST change is mainly controlled by subsurface processes. In the fast-wave limit, the ocean dynamics adjust more rapidly than SST, so SST change is mainly controlled by surface processes. With this theory, eastward or westward propagating and stationary SST modes can mix with ocean dynamics modes to form mixed SST/ocean dynamics modes.

Given the increasing complexity of precedent models and the finding that the meridional scale of coupled oscillations exceeds what can be explained using an oceanic equatorial Rossby radius of deformation, we have been considering analytically tractable models in an attempt to gain insights on coupled equatorial wave mode properties. The starting point has been Hirst (1986). By assuming zonal wind stress and SST anomalies to be proportional, Wang and Weisberg (1994a) obtained an eastward propagating mode whose stability depends upon the zonal phase lag between the wind stress and SST anomalies. Omitting the phase lag and assuming equal coefficient values for Rayleigh friction/Newtonian cooling and thermal damping, Wang and Weisberg (1994b) then obtained neutral modes over the full range of equatorial waves. The effects of cou-

pling were found to increase with decreasing frequency, with the Rossby and Kelvin modes transforming into westward and eastward slow modes, respectively, and with the meridional scale of these modes increasing beyond the oceanic equatorial Rossby radius of deformation. Here we relax the equal coefficient value and the zero phase lag assumptions, and examine how the coupled Rossby and Kelvin modes may coexist with westward and eastward slow modes, how the coupled equatorial modes may merge, separate, and be destabilized by varying model parameters, and how their meridional scales are affected. Section 2 presents the coupled model by assuming that the zonal wind stress and SST perturbations are proportional and separated zonally. Section 3 develops analytical solutions for both westward and eastward propagating modes, the properties of which are explored in section 4. A discussion and summary are then given in section 5.

2. The model formulation

The ocean dynamic equations are those of a linear, equatorial β -plane, reduced-gravity model with a long-wave approximation, perturbed about a basic state of rest by the zonal component of wind stress τ^x . The upper layer has density ρ and mean depth H_0 ; the lower layer has slightly higher density, and is infinitely deep and motionless. Momentum and mass are thus governed by

$$\frac{\partial u}{\partial t} - \beta y v = -g' \frac{\partial h}{\partial x} + \frac{\tau^x}{\rho H_0} - \gamma u \quad (2.1)$$

$$\beta y u = -g' \frac{\partial h}{\partial y} \quad (2.2)$$

$$\frac{\partial h}{\partial t} + H_0 \left(\frac{\partial u}{\partial x} + \frac{\partial v}{\partial y} \right) = -\gamma h, \quad (2.3)$$

where u and v are the velocity components in the zonal (x) and meridional (y) directions; h is the upper-layer thickness perturbation; t is time; g' is the reduced gravity; β is the gradient in planetary vorticity; and γ is a coefficient representing Rayleigh friction and Newtonian cooling, providing dissipation in the momentum and mass equations, respectively.

The long-wave approximation is valid if the zonal scale is large compared with the meridional scale. Consistent with this, τ^y is neglected because ENSO-related wind perturbations are primarily zonal and τ^y has a smaller effect at large zonal scales than does τ^x . This approximation removes inertial–gravity, Rossby–gravity, and short Rossby modes from the system (shown to be unaffected by coupling in Wang and Weisberg 1994b) while maintaining the important Kelvin and long Rossby modes (e.g., Hirst 1988; Wakata and Sarachik 1991, 1994; Jin and Neelin 1993a). A long-wave approximation using equal values for Ray-

TABLE 1. Values for the basic parameters.

Parameter	Value
H_0	200 m
c	2 m s^{-1}
β	$2.29 \times 10^{-11} \text{ m}^{-1} \text{ s}^{-1}$
μ	$0.85 \times 10^{-7} \text{ m s}^{-2} \text{ K}^{-1}$
σ	$5.0 \times 10^{-9} \text{ K m}^{-1} \text{ s}^{-1}$
η	$-5.0 \times 10^{-7} \text{ K m}^{-1}$
α	1 yr^{-1}
γ	1 yr^{-1}
θ	0

leigh friction and Newtonian cooling has been shown to be valid by Yamagata (1985).

The thermodynamics controlling the variations in SST anomaly (T) are a trade-off between ocean processes and surface heat fluxes. The ocean processes are lumped into a term proportional to the upper-layer thickness perturbation except for zonal advection, which is treated separately. Thus, the thermodynamic equation has the form of the Hirst (1986) Model III:

$$\frac{\partial T}{\partial t} + \eta u = \sigma h - \alpha T, \quad (2.4)$$

where σ is the warming parameter, η is the specified zonal SST gradient, and α is a thermal damping coefficient. The simplified SST equation (2.4) with constant parameters, rather than a more complicated SST equation, is chosen herein for analytical tractability. The model limitations will be discussed later.

To form a coupled ocean-atmosphere system, τ^x must be specified in terms of ocean variables. Gill (1980) noted that the response of a tropical atmosphere to SST-induced heating has a significant east-west asymmetry with the westerly winds to the west of the SST-induced heating being more intense than the easterly winds to the east of it. Observations confirm that westerly wind anomalies are located to the west of positive SST anomalies (e.g., Zebiak 1993; Latif and Barnett 1995), suggesting that τ^x may be parameterized as a linear function of T lagged by a zonal phase angle θ ; that is,

$$\tau^x(x, y, t) = \rho \mu H_0 e^{i\theta} T(x, y, t), \quad (2.5)$$

where μ is the ocean-atmosphere coupling coefficient and $i = \sqrt{-1}$.

A related assumption with differing modifications has been used by Battisti and Hirst (1989), Schopf and Suarez (1990), Cane et al. (1990), and Neelin (1991). This assumption also forms the basis for coupling an OGCM with a statistical atmosphere, such as Barnett et al. (1993), wherein the wind stress was taken proportional to a linear combination of SST EOF modes. It must be recognized, however, that the τ^x specification of Eq. (2.5) is unrealistic in several ways: 1) it omits τ^y , 2) it requires that τ^x

have the same meridional structure as T , and 3) it assumes spatially uniform coupling. A numerical examination of a similar system of equations, but omitting the long-wave approximation and using a Gill (1980) atmosphere (Wang and Weisberg 1994a), has shown that τ^y is much smaller than τ^x and that the correlation between τ^x and T is positive equatorward of 14° . The first finding is consistent with the long-wave approximation used here and the correlation is consistent with the structure found by Barnett et al. (1993) when correlating their statistical atmosphere τ^x with observed τ^x . In reality, the coupling coefficient μ is not homogeneous, nonlinear effects are important, and the correlation between τ^x and T does diminish poleward from the equator. Thus, spatially uniform coupling is erroneous, but this limitation is tempered by that the gravest mode ocean (atmosphere) equatorial waves are forced primarily by winds (heating) near the equator. With these limitations noted, the basic model parameters are shown in Table 1. These values were chosen to give realistic wind stress and SST perturbations for observed environmental conditions.

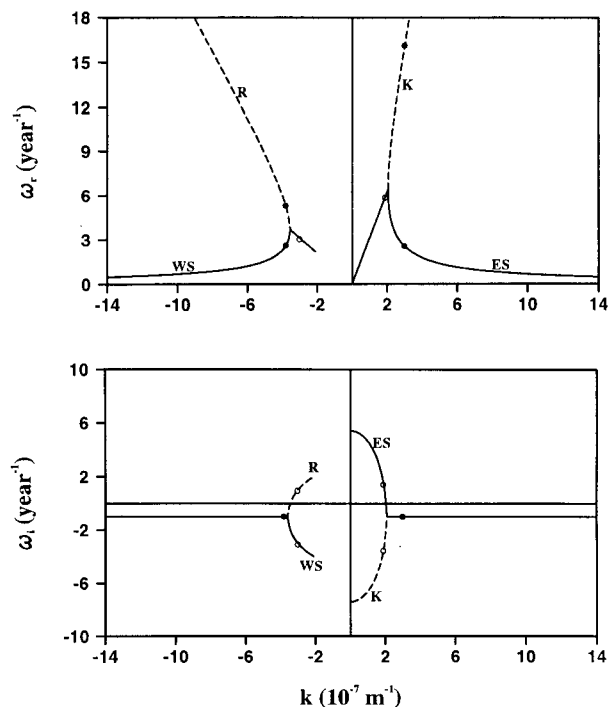


FIG. 1. Frequency ω_r and growth rate ω_i of coupled equatorial modes as a function of wavenumber k , with the model parameters of Table 1. The negative (positive) values of k represent westward (eastward) propagating modes. The dashed lines represent the gravest coupled Rossby or Kelvin (R or K) modes, and the solid lines represent the gravest westward or eastward slow (WS or ES) modes. The solid dots and open circles denote the points at which horizontal eigenfunction structures are presented in the subsequent figures.

3. Solutions of coupled equatorial modes

a. Westward propagating modes

We assume wavelike solutions to Eqs. (2.1)–(2.5) of the form

$$\begin{pmatrix} u(x, y, t) \\ v(x, y, t) \\ h(x, y, t) \\ T(x, y, t) \\ \tau^x(x, y, t) \end{pmatrix} = \begin{pmatrix} u(y) \\ v(y) \\ h(y) \\ T(y) \\ \rho\mu H_0 e^{i\theta} T(y) \end{pmatrix} e^{i(kx - \omega t)}, \quad (3.1)$$

where k is a real zonal wavenumber and ω is a complex frequency with real (ω_r) and imaginary (ω_i) parts representing the frequency and the growth rate, respectively. With ω_r taken to be positive the direction of zonal phase propagation is determined by the sign of k . Substituting Eq. (3.1) into Eqs. (2.1–4) yields

$$(\gamma - i\omega)u - \beta yv = -ikg'h + \mu e^{i\theta}T \quad (3.2)$$

$$\beta yu = -g' \frac{dh}{dy} \quad (3.3)$$

$$(\gamma - i\omega)h + ikH_0u + H_0 \frac{dv}{dy} = 0 \quad (3.4)$$

$$(\alpha - i\omega)T + \eta u = \sigma h. \quad (3.5)$$

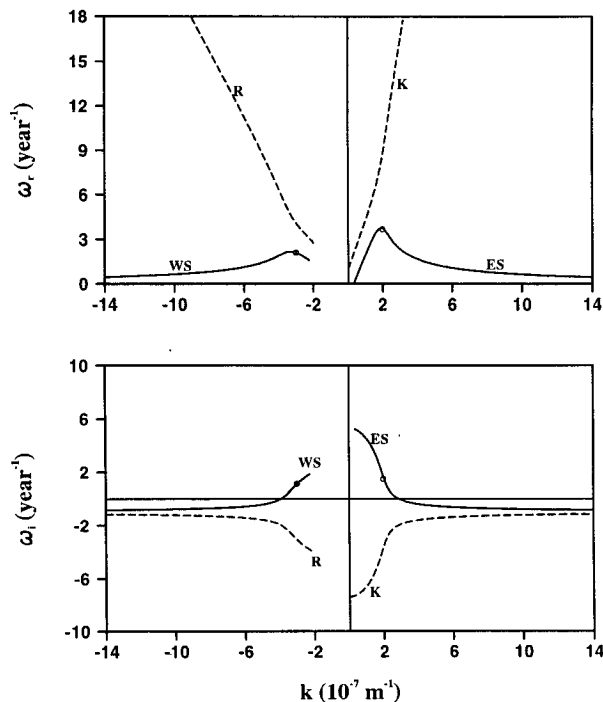


FIG. 2. As in Fig. 1 but for $\theta = 0.1\pi$.

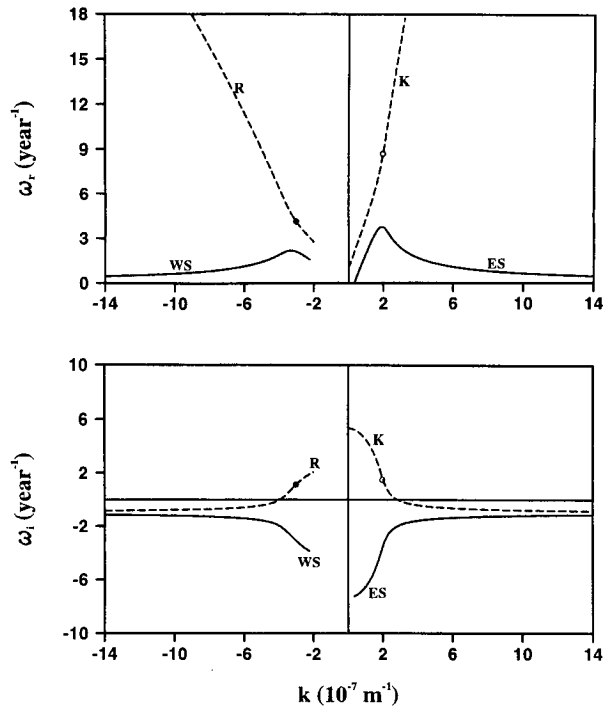


FIG. 3. As in Fig. 1 but for $\theta = -0.1\pi$.

Eliminating u , h , and T results in the single equation for v :

$$\frac{d^2v}{dy^2} + Ay \frac{dv}{dy} + B(1 - Cy^2)v = 0, \quad (3.6)$$

where

$$A \equiv \frac{H_0\beta\mu\sigma e^{i\theta}}{c^2[(\gamma - i\omega)(\alpha - i\omega) + \mu\eta e^{i\theta}]} \quad (3.7a)$$

$$B \equiv \frac{ikc^2\beta(\alpha - i\omega)}{c^2[(\gamma - i\omega)(\alpha - i\omega) + \mu\eta e^{i\theta}]} \quad (3.7b)$$

$$C \equiv \frac{\beta(\gamma - i\omega)}{ikc^2} \quad (3.7c)$$

and $c = (g'H_0)^{1/2}$ is the ocean equatorial Kelvin wave speed. Using the substitution

$$v(y) = \tilde{v}(\xi) \exp\left(\frac{D\xi^2}{2}\right), \quad (3.8a)$$

$$\xi = -i\left(\frac{A}{2D}\right)^{1/2} y, \quad D = \frac{1}{(1 + 4BC/A^2)^{1/2}}, \quad (3.8b)$$

Eq. (3.6) transforms to

$$\frac{d^2\tilde{v}}{d\xi^2} + \left(D - \frac{2DB}{A} - \xi^2\right)\tilde{v} = 0. \quad (3.9)$$

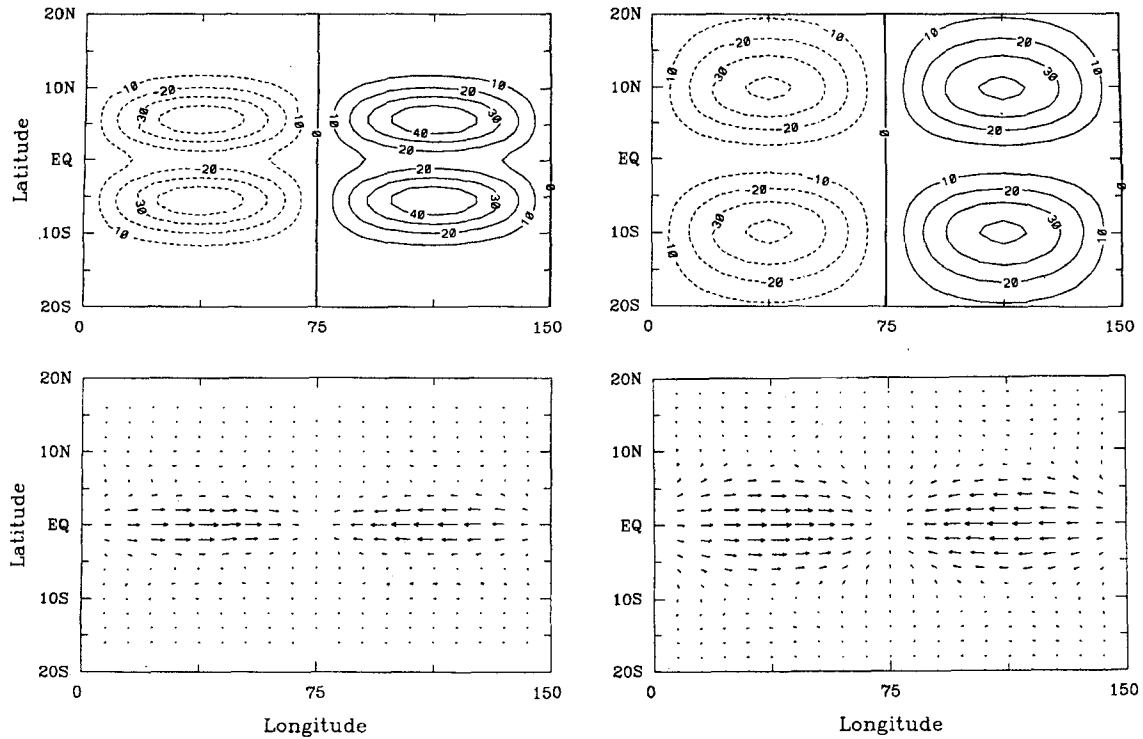


FIG. 4. The horizontal eigenfunction structures for the gravest westward propagating modes with $k = -3.8 \times 10^{-7} \text{ m}^{-1}$ denoted by the solid dots in the dispersion plane of Fig. 1 and the model parameters of Table 1. The left-hand plates give the thermocline height and the current vector anomalies for the coupled Rossby mode and the right-hand plates give the counterpart fields for westward slow mode. The meridional/zonal dimensions are in latitude/longitude degrees and the zonal dimension spans one wavelength.

Subject to the dispersion relationship

$$D - \frac{2DB}{A} = 2n + 1, \quad n = 1, 2, \dots, \quad (3.10)$$

Eq. (3.9) has analytical solutions

$$\tilde{v}(\xi) = C_1 \exp(-\xi^2/2) H_n(\xi), \quad (3.11)$$

where C_1 is a dimensional constant and $H_n(\xi)$ is the n th-order Hermite polynomial. Substituting Eq. (3.11) into Eq. (3.8a) and using the dispersion relationship yields

$$v(y) = C_1 \exp\left[-\frac{nA + B}{2(2n + 1)} y^2\right] \times H_n[-i(A/2D)^{1/2}y]. \quad (3.12)$$

This solution is bounded [$v(y) \rightarrow 0$ as $y \rightarrow \pm\infty$] when $\text{Re}(nA + B) > 0$. Using Eqs. (3.7a-c) and (3.8b) allows the dispersion relationship to be rewritten as

$$\begin{aligned} [H_0\sigma\mu e^{i\theta} - i2kc^2(\alpha - i\omega)] / \{ (H_0\sigma\mu e^{i\theta})^2 \\ + 4c^2(\alpha - i\omega)(\gamma - i\omega)[(\alpha - i\omega)(\gamma - i\omega) + \mu\eta e^{i\theta}]^{1/2} \} \\ = 2n + 1, \quad (3.13) \end{aligned}$$

and the ensuing meridional eigenfunctions, subject to the constraint $\text{Re}(nA + B) > 0$, are

$$v(y) = C_1 \exp\left[-\frac{nA + B}{2(2n + 1)} y^2\right] \times H_n[-i(A/2D)^{1/2}y] \quad (3.14)$$

$$u(y) = \frac{1}{\Pi} \left\{ (\alpha - i\omega)(\gamma - i\omega)\beta y v - [H_0\sigma\mu e^{i\theta} - ikc^2(\alpha - i\omega)] \frac{dv}{dy} \right\} \quad (3.15)$$

$$h(y) = -\frac{H_0}{\Pi} \left\{ ik(\alpha - i\omega)\beta y v + [(\gamma - i\omega)(\alpha - i\omega) + \mu\eta e^{i\theta}] \frac{dv}{dy} \right\}, \quad (3.16)$$

where

$$T(y) = -\frac{1}{\Pi} \left\{ [iH_0\sigma k + \eta(\gamma - i\omega)]\beta y v + [H_0\sigma(\gamma - i\omega) + ikc^2\eta] \frac{dv}{dy} \right\}, \quad (3.17)$$

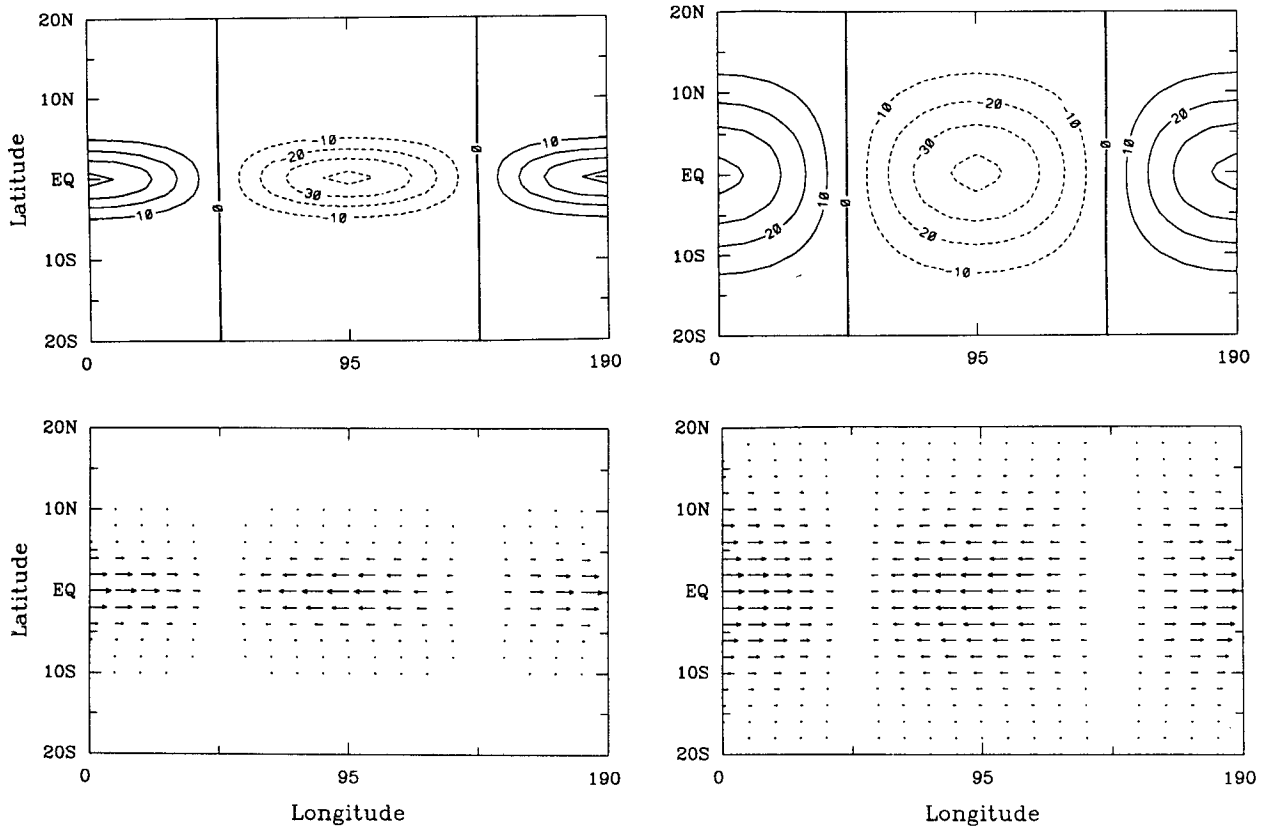


FIG. 5. The horizontal eigenfunction structures for eastward propagating modes with $k = 3.0 \times 10^{-7} \text{ m}^{-1}$ denoted by the solid dots in the dispersion plane of Fig. 1 and the model parameters of Table 1. The left-hand plates give the thermocline height and the current vector anomalies for the coupled Kelvin mode and the right-hand plates give the counterpart fields for eastward slow mode. The meridional/zonal dimensions are in latitude/longitude degrees and the zonal dimension spans one wavelength.

where

$$\Pi = (\gamma - i\omega)[(\gamma - i\omega)(\alpha - i\omega) + \mu\eta e^{i\theta}] + k^2 c^2 (\alpha - i\omega) + ikH_0\sigma\mu e^{i\theta}. \quad (3.18)$$

To obtain the velocity, thermocline thickness, and SST anomalies, Eqs. (3.14–17) are multiplied by $\exp[i(kx - \omega t)]$.

b. Eastward propagating modes

Like conventional equatorial waves, eastward propagating modes exist with v identically zero. Setting $v = 0$ and substituting Eq. (3.1) into Eqs. (2.1–4) yields

$$(\gamma - i\omega)u + ikg'h - \mu e^{i\theta}T = 0 \quad (3.19)$$

$$\beta y u = -g' \frac{dh}{dy} \quad (3.20)$$

$$ikH_0 u + (\gamma - i\omega)h = 0 \quad (3.21)$$

$$\eta u - \sigma h + (\alpha - i\omega)T = 0. \quad (3.22)$$

The algebraic Eqs. (3.19), (3.21), and (3.22) have solutions for u , h , and T only when

$$(\gamma - i\omega)^2 + k^2 c^2 + \frac{iH_0\mu\sigma k e^{i\theta}}{\alpha - i\omega} + \frac{(\gamma - i\omega)\mu\eta e^{i\theta}}{\alpha - i\omega} = 0, \quad (3.23)$$

which is the dispersion relationship for the eastward propagating modes and their associated meridional eigenfunctions are

$$h(y) = C_2 \exp\left[-\frac{\beta(\omega + i\gamma)}{2kc^2} y^2\right] \quad (3.24)$$

$$u(y) = \frac{C_2(\omega + i\gamma)}{kH_0} \times \exp\left[-\frac{\beta(\omega + i\gamma)}{2kc^2} y^2\right] \quad (3.25)$$

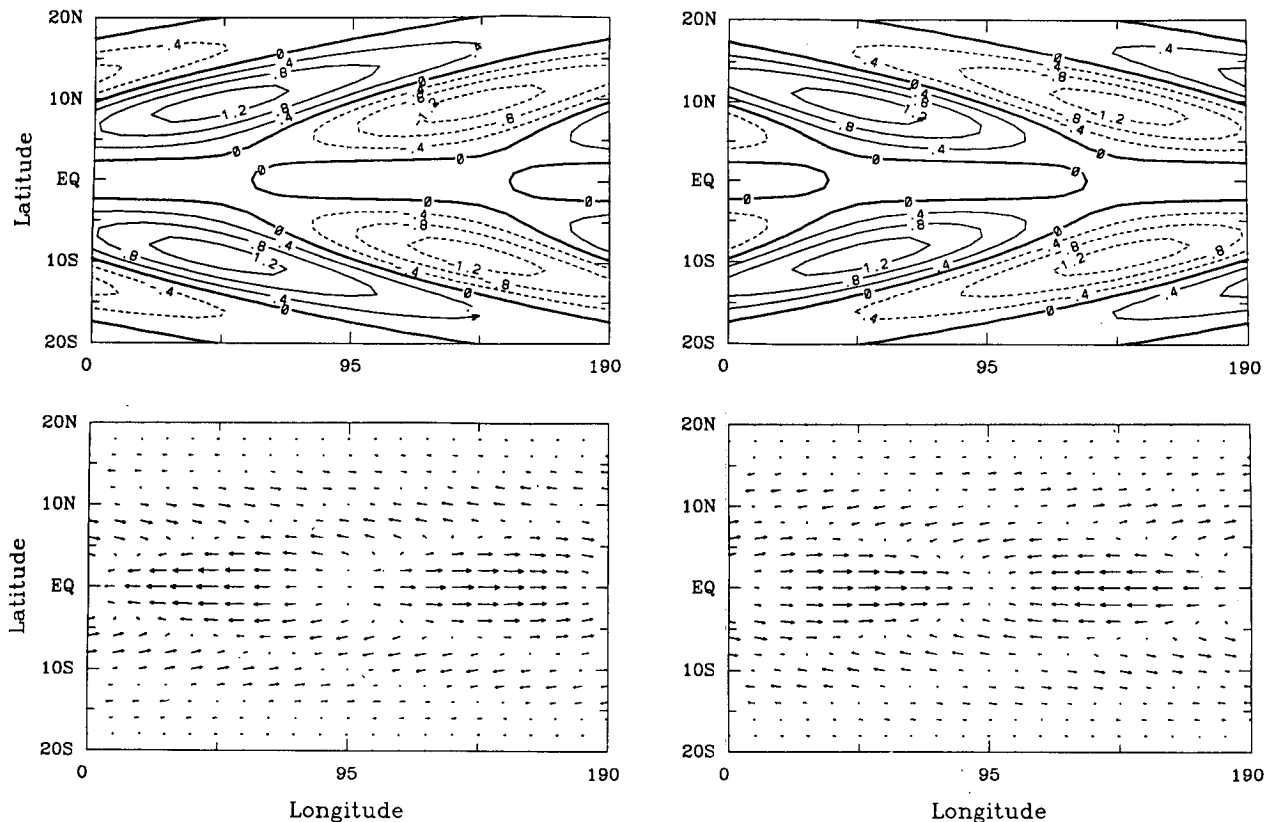


FIG. 6. As in Fig. 4 but for the eigenfunctions of the SST and the current vector anomalies with $k = -3.0 \times 10^{-7} \text{ m}^{-1}$ denoted by the open circles in the dispersion plane of Fig. 1.

$$T(y) = \frac{C_2[H_0 k \sigma - \eta(\omega + i\gamma)]}{kH_0(\alpha - i\omega)} \times \exp\left[-\frac{\beta(\omega + i\gamma)}{2kc^2} y^2\right], \quad (3.26)$$

where C_2 is a dimensional constant.

4. Analysis of the solutions

a. The basic features

The horizontal structure of the modes can be described by taking the real part of Eqs. (3.1). The meridional velocity component, for example, may be expressed as

$$v(x, y, t) = \text{Re}[v(y)e^{i(kx - \omega t)}] \\ = \sqrt{v_r^2 + v_i^2} \cos(kx - \omega t + \varphi), \quad (4.1)$$

where v_r and v_i are the real and imaginary parts of $v(y)$ and $\varphi = \tan^{-1}v_i/v_r$. Unlike uncoupled equatorial waves, both the wave amplitude and phase are functions of y .

The frequency ω_r and growth rate ω_i of the coupled equatorial modes as a function of wavenumber k using

the model parameters of Table 1 are shown in Fig. 1. The negative (positive) values of k represent westward (eastward) propagating modes; the dashed lines represent the gravest coupled Rossby or Kelvin (R or K) modes and the solid lines represent the gravest westward or eastward slow (WS or ES) modes. For the westward propagating modes, only the gravest ($n = 1$) modes will be discussed since higher meridional modes behave similarly. In the dispersion plane the coupled Rossby and Kelvin modes are distinguished from the westward and eastward slow modes in that the wavenumber magnitude increases with increasing frequency for the former and decreases with increasing frequency for the latter. At the transition points where these modes merge there is a branch within which the frequencies of the coupled Rossby (Kelvin) and the westward (eastward) slow modes are the same, as shown by the dashed line overlapping the solid line. The merge point for the westward propagating modes occurs at relatively lower frequency and larger k than for the eastward propagating modes. The decay rates of all equatorial modes are the uncoupled oceanic damping rate of -1 yr^{-1} for $|k|$ exceeding the merge point values. However, for smaller $|k|$, the coupled Rossby (Kelvin) mode is unstable (stable), whereas the westward (east-

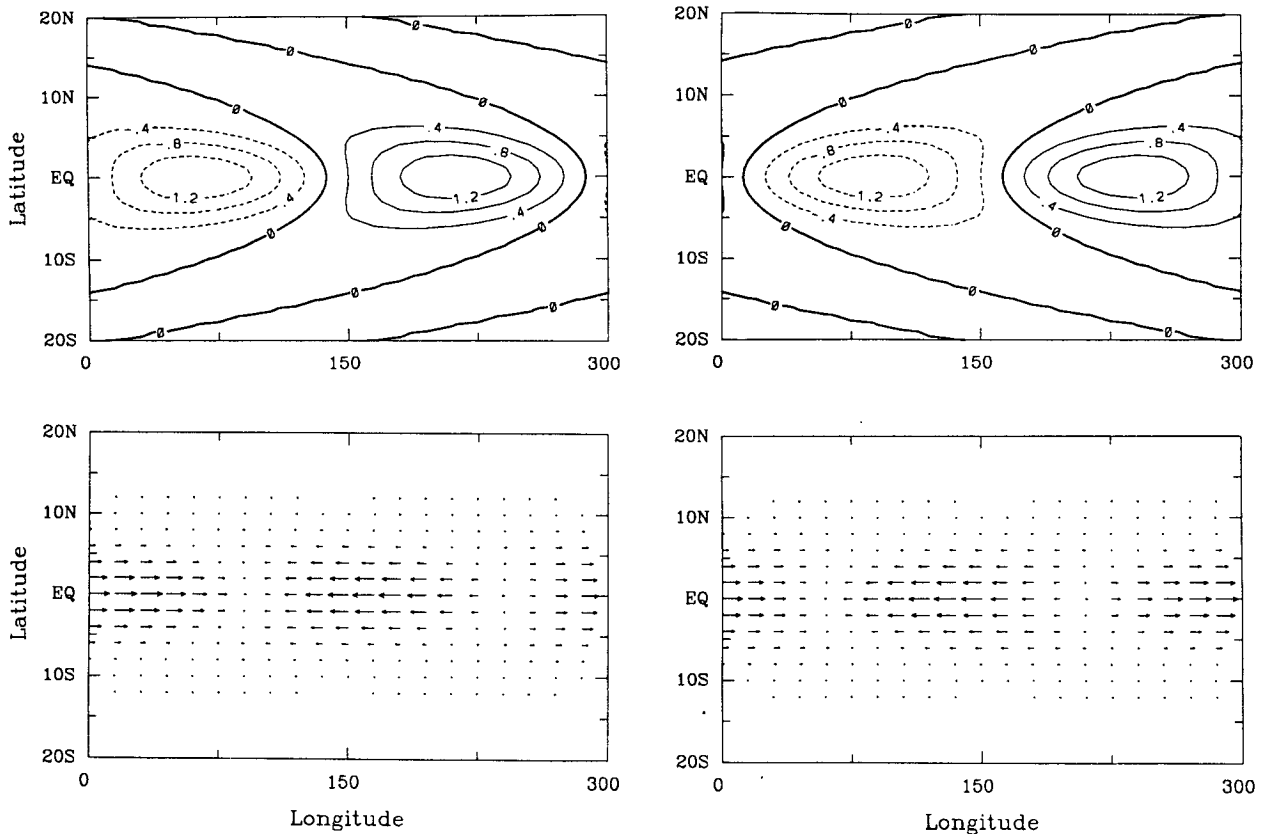


FIG. 7. As in Fig. 5 but for the eigenfunctions of the SST and the current vector anomalies, with $k = 1.9 \times 10^{-7} \text{ m}^{-1}$ denoted by the open circles in the dispersion plane of Fig. 1.

ward) slow mode is stable (unstable). Upon merging, the coupled Rossby (Kelvin) and westward (eastward) slow modes split into two branches: one growing and one decaying. It is noted that the dispersion relationship does not extend to the origin for the westward propagating modes owing to the constraint on (3.12) that $\text{Re}(nA + B) > 0$.

There is no zonal phase difference in Fig. 1: $\theta = 0$. The effects of positive and negative zonal phase differences θ between the τ^x , and SST anomalies are shown in Figs. 2 and 3, respectively, using the model parameters of Table 1, but with $\theta = 0.1\pi$ or $\theta = -0.1\pi$. Positive or negative θ indicates that the τ^x anomaly is located to the west or east of the SST anomaly, respectively. In comparison with Fig. 1, the coupled Rossby and Kelvin modes no longer merge with the westward and eastward slow modes. The frequency of the modes is independent of the sign of θ , whereas the stability properties reverse sign with θ . Positive θ tends to destabilize the westward and eastward slow modes, while tending to damp the coupled Rossby and Kelvin modes. Negative θ reverses these tendencies; that is, the coupled Rossby and Kelvin modes are destabilized, whereas the westward and eastward slow modes are

damped. This means that, if westerly winds are to the west (east) of the SST anomaly, westward and eastward slow modes (coupled Rossby and Kelvin modes) are destabilized. In nature, warm waters induce atmospheric convergence, resulting in westerly (easterly) winds to the west (east) of a warm anomaly (e.g., Gill 1980). Therefore, westerlies to the west of a positive SST anomaly are more realistic than westerlies to the east, implying that destabilization tends to favor the slow modes.

The horizontal eigenfunction's structures for the gravest westward (with $k = -3.8 \times 10^{-7} \text{ m}^{-1}$) and eastward (with $k = 3.0 \times 10^{-7} \text{ m}^{-1}$) propagating modes using the model parameters of Table 1 are shown in Figs. 4 and 5, respectively. This choice of wavenumbers, with magnitudes larger than the merge point wavenumbers, allows us to compare the relative structures between the westward Rossby and westward slow modes and between the eastward Kelvin and eastward slow modes. The associated points in the dispersion plane are denoted by solid dots in Fig. 1, the frequency of the slow modes being 2.5 yr^{-1} and all modes being neutral if the uncoupled damping rate is factored out. The left-hand plates give the thermocline height

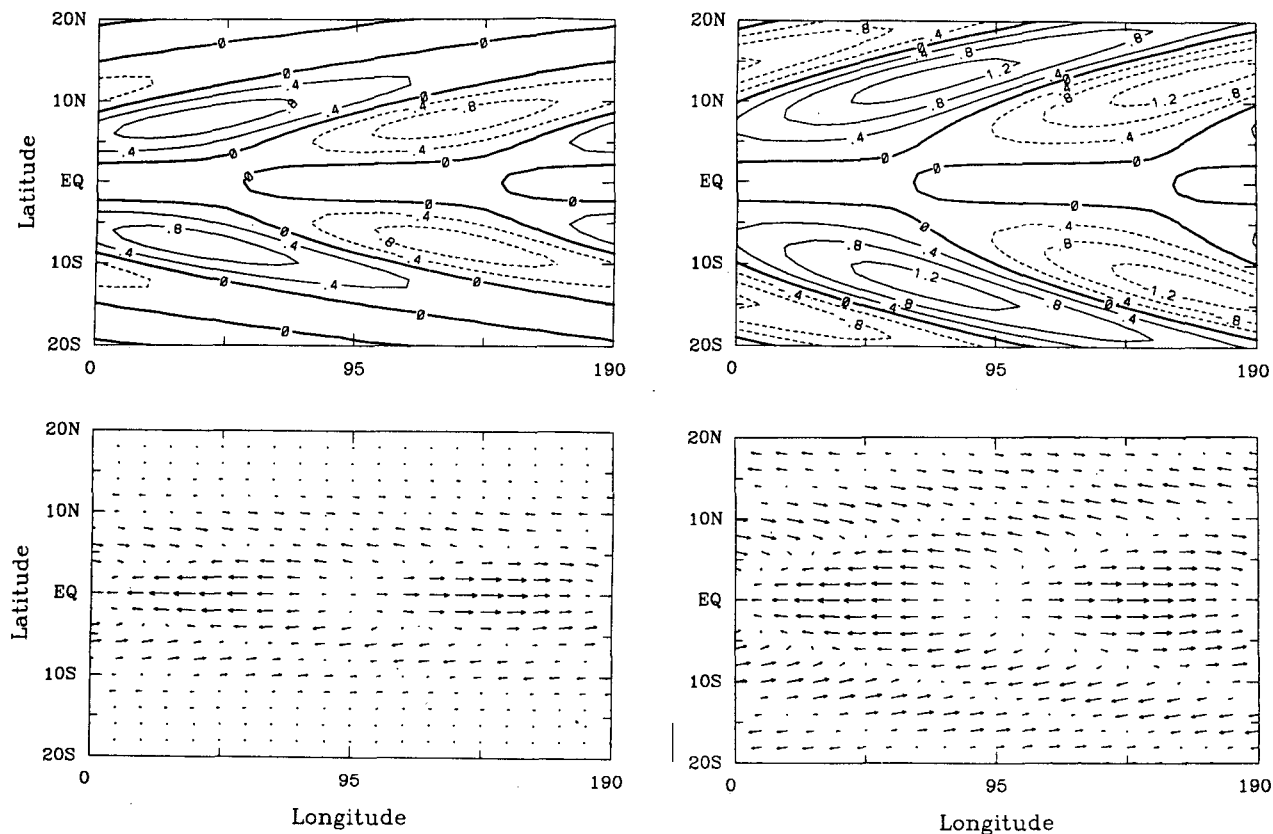


FIG. 8. The horizontal eigenfunction structures for the gravest unstable westward propagating modes with $k = -3.0 \times 10^{-7} \text{ m}^{-1}$ denoted by the solid dots in Figs. 2 and 3. The left-hand plates give the SST and the current vector anomalies for unstable Rossby mode and the right-hand plates give the counterpart fields for unstable westward slow mode. The meridional/zonal dimensions are in latitude/longitude degrees and the zonal dimension spans one wavelength.

and the current vector anomalies for the coupled Rossby (or Kelvin) mode and the right-hand plates give the counterpart fields for westward (or eastward) slow mode. The meridional/zonal dimensions are in latitude/longitude degrees and the zonal dimension spans one wavelength. The structures are the same as those of the coupled modes at 2.5 yr^{-1} frequency shown in Wang and Weisberg (1994b). Note that the meridional scales for the slow modes are much larger than the oceanic equatorial Rossby radius of deformation. For example, the maximum height anomalies for the westward slow mode are centered at $\pm 10^\circ$ from the equator. Similarly, the zonal jets for these slow modes expand to become tropical, rather than equatorial, features. The meridional scales of the coupled Rossby and Kelvin modes, while smaller than their slow mode counterparts, are larger than those for uncoupled equatorial waves (Matsuno 1966).

Other interesting points for eigenfunction comparisons are those for which the coupled Rossby or Kelvin modes have merged with their slow mode counterparts, for example, at $k = -3.0 \times 10^{-7} \text{ m}^{-1}$ and $k = 1.9 \times 10^{-7} \text{ m}^{-1}$ denoted by open circles in the dispersion

plane of Fig. 1. The horizontal structures for the gravest westward and eastward propagating modes using the model parameters of Table 1 are shown in Figs. 6 and 7, respectively. The left-hand plates give the SST and the current vector anomalies for the coupled unstable Rossby (or stable Kelvin) mode and the right-hand plates give the counterpart fields for stable westward (or unstable eastward) slow mode. Again, all these modes have a much broader meridional scale than for uncoupled equatorial waves. For the westward propagating modes, the maximum SST anomalies are centered at $\pm 9^\circ$ from the equator; additionally, with a meridional phase gradient, flows now reverse with latitude. Note that the current vectors for the unstable Rossby mode have opposite sign to those for the stable westward slow mode. Also, owing to this meridional phase gradient (which is imparted by the imaginary part of ω), the SST contours for the unstable Rossby mode and the stable westward slow mode tilt in opposite directions with latitude. For the eastward propagating modes, the current vector and SST anomalies have similar structures except for a zonal phase shift and an oppositely directed tilt. By comparing the rel-

ative positions of the current and SST anomalies for the unstable eastward slow mode (and the stable Kelvin mode), it is seen that the eastward (westward) SST anomaly shift results in a positive (negative) correlation between the wind stress (proportional to SST) and the current. With westerlies (easterlies) overlying oceanic eastward (westward) current for the coupled Rossby and eastward slow modes, the necessary condition for instability (Yamagata 1985) of positive correlation between the wind stress and current is satisfied, enabling these modes to grow. In contrast, the correlation between the wind stress and current is negative for the coupled Kelvin and the westward slow modes, so these modes decay.

The effects of θ on the horizontal structures of the eigenfunctions for the gravest unstable westward (with $k = -3.0 \times 10^{-7} \text{ m}^{-1}$ denoted by solid dots in Figs. 2 and 3) and unstable eastward (with $k = 2.0 \times 10^{-7} \text{ m}^{-1}$ denoted by open circles in Figs. 2 and 3) propagating modes with θ either 0.1π or -0.1π and using the other parameters of Table 1 are shown in Figs. 8 and 9, respectively. The left-hand plates give the SST and the current vector anomalies for the unstable Rossby (or Kelvin) mode and the right-hand plates give the counterpart fields for unstable westward (or eastward) slow

mode. The meridional scale increase for coupled modes is again noted. Furthermore, the meridional scales for the slow modes (that occur at lower frequency) are larger than for the coupled unstable Rossby or Kelvin modes, reflecting the frequency dependence of the meridional scale for coupled modes in this model (Wang and Weisberg 1994b). As shown in the next section, the frequencies of the slow modes (coupled Rossby and Kelvin modes) decrease (increase) with increasing $|\theta|$. Therefore, the meridional scales of the slow modes (coupled Rossby and Kelvin modes) will increase (decrease) with increasing $|\theta|$.

The eigenfunctions presented herein share some similarities with observations. For example, the SST eigenfunctions for unstable eastward Kelvin or slow modes are consistent with the SST pattern of the leading canonical correlation analysis mode of Latif and Barnett (1995, Fig. 4a) in that the SST contours tilt in the same direction (northeastward) and with broad meridional scale.

The fast-wave and fast-SST limits of Neelin (1991) and Jin and Neelin (1993a) also can be performed by introducing an additional parameter δ in the time derivatives of Eqs. (2.1) and (2.3), which measures the ratio of ocean dynamics to SST adjustment times. Two limits are represented by small and large δ , respec-

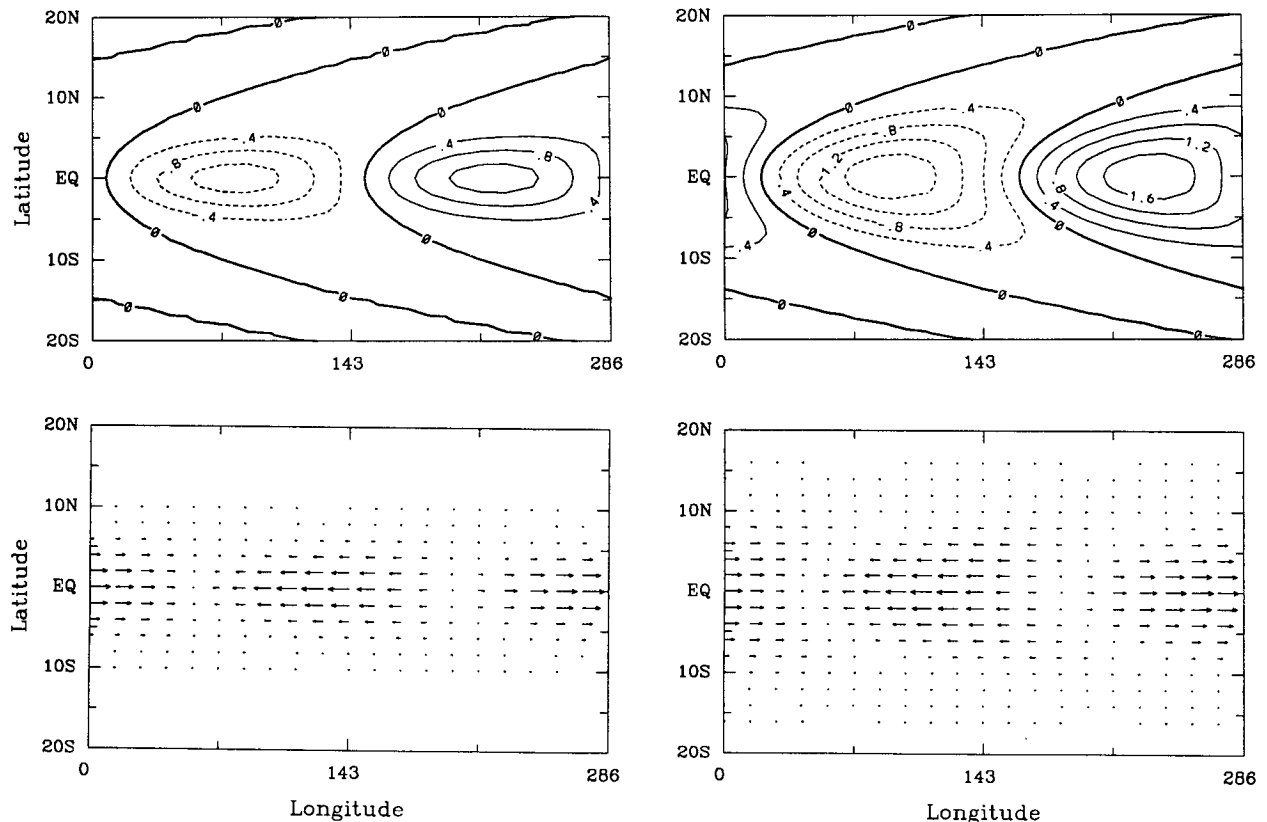


FIG. 9. As in Fig. 8 but for unstable eastward propagating modes with $k = 2.0 \times 10^{-7} \text{ m}^{-1}$ denoted by the open circles in Figs. 2 and 3.

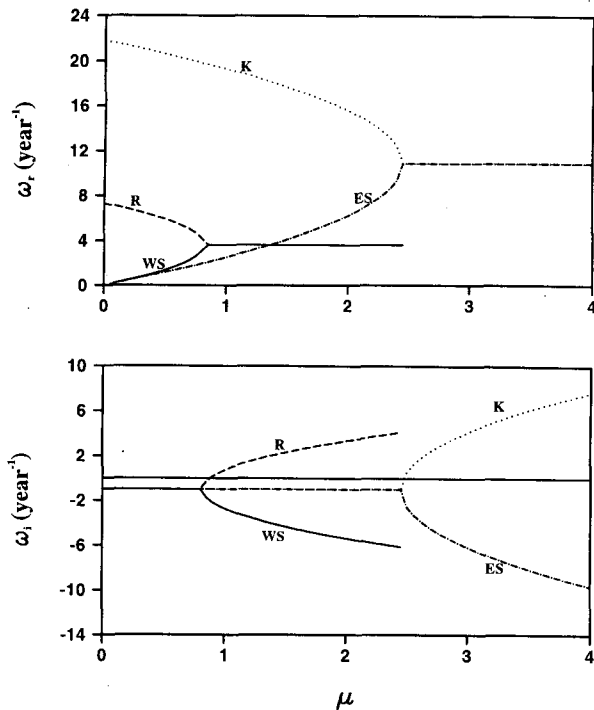


FIG. 10. Frequency ω_r and growth rate ω_i of coupled equatorial modes as a function of coupling coefficient μ ($10^{-7} \text{ m s}^{-2} \text{ K}^{-1}$) with $k = \pm 3.5 \times 10^{-7} \text{ m}^{-1}$ (positive and negative values of k represent eastward and westward propagating modes, respectively) and other model parameters of Table 1. The solid and dashed lines represent westward slow (WS) mode and coupled Rossby (R) mode, respectively. The dotted-dashed and dotted lines represent eastward slow (ES) mode and coupled Kelvin (K) mode, respectively.

tively. In this model, the fast-wave limit filters the coupled Rossby and Kelvin modes out of the system, leaving only the westward and eastward slow modes which are unstable at small wavenumber. The variations of these coupled slow modes depend upon the time derivative of the SST equation instead of that in the dynamical equations, demonstrating that instability can exist in this coupled system without Rossby or Kelvin modes. Unlike the fast-wave limit, the coupled Rossby and Kelvin modes coexist with the slow modes in the fast-SST limit. However, the frequency and growth rate magnitudes for both the coupled Rossby and Kelvin modes are largely reduced. As δ increases from fast-wave limit toward fast-SST limit values (0 to large), the frequencies of both the coupled Rossby and Kelvin modes approach those of the slow modes. This may explain why the ocean dynamics modes and the slow SST modes merge into complicated mixed modes in Jin and Neelin (1993a).

b. Dependence on model parameters

Given the dispersion relationship and eigenfunction dependencies upon ill-defined model parameters, the

following sensitivity studies are presented over physically reasonable parameter ranges (e.g., the range of η follows from the maximum large-scale zonal SST gradient).

1) THE PARAMETERS μ , σ , AND η

The effects of the coupling coefficient μ , the warming coefficient σ , and the zonal mean SST gradient η on the frequency and stability of the coupled equatorial modes using the model parameters of Table 1 are shown in Figs. 10, 11, and 12, respectively. The trivial result of zero frequency for the slow modes when $\mu = 0$ and $\sigma = 0$ is consistent with the slow modes owing their existence to air-sea coupling and warming processes. Unlike μ and σ the existence of the slow modes is not dependent upon η , as shown by Wang and Weisberg (1994b).

The frequency of the slow modes increases with increasing μ until merging with the coupled Rossby and Kelvin modes. The coupled Rossby and Kelvin modes, which begin as the conventional Rossby and Kelvin modes for $\mu = 0$, are strongly modified by coupling. The frequencies of the coupled Rossby and Kelvin modes decrease with increasing μ until merging with the slow modes. After merging, the frequency of these modes is independent of μ except for the coupled Rossby and the westward slow modes upon reaching the eigenfunction constraint $\text{Re}(nA + B) > 0$. Before

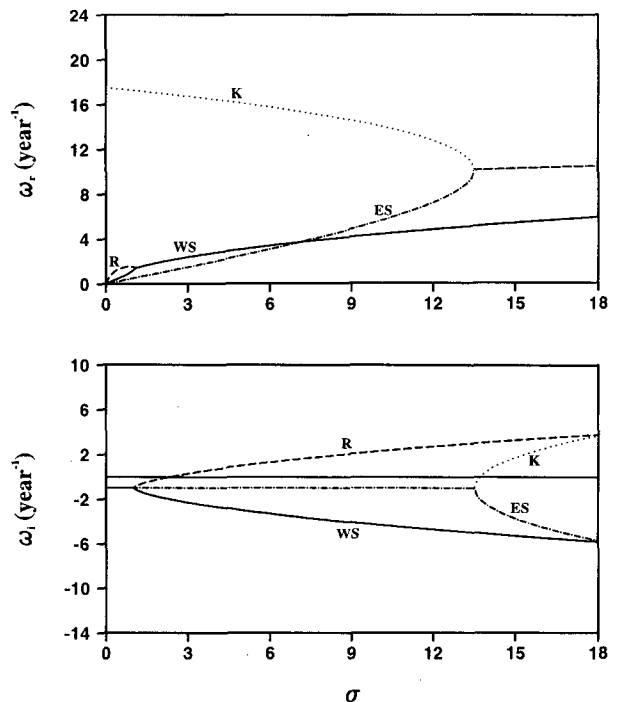


FIG. 11. As in Fig. 10 but as a function of warming coefficient σ ($10^{-9} \text{ K m}^{-1} \text{ s}^{-1}$) with $k = \pm 3.0 \times 10^{-7} \text{ m}^{-1}$.

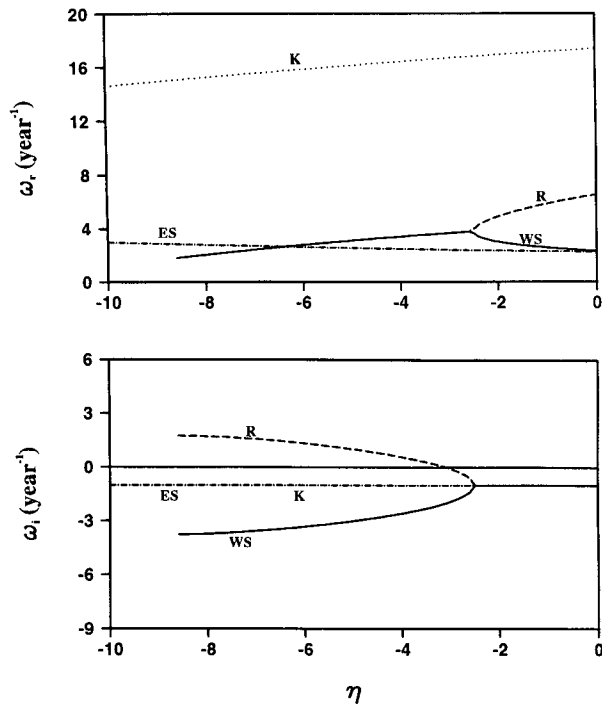


FIG. 12. As in Fig. 10 but as a function of zonal mean SST gradient η (10^{-7} K m^{-1}) with $k = \pm 3.0 \times 10^{-7} \text{ m}^{-1}$.

merging, the decay rate for all modes is the uncoupled damping rate of -1 yr^{-1} . After merging, the coupled Rossby and Kelvin modes can be destabilized, whereas the slow modes decay more rapidly. Thus, upon merging, coupled Rossby (Kelvin) and westward (eastward) slow modes develop two branches: one growing and the other decaying. Destabilization of the coupled Rossby or Kelvin modes and stabilization of the slow modes by increasing μ results from the induced positive and negative correlations between the winds and currents of these modes, respectively, for this parameter choice.

The effects of σ on the coupled mode's frequency and stability are similar to those of μ . With increasing σ the coupled Rossby and Kelvin modes merge with the westward and eastward slow modes. For the coupled Rossby mode and the slow modes frequency increases with increasing σ . Before merging with the eastward slow mode the coupled Kelvin mode frequency decreases with increasing σ , whereas after merging it increases slowly with σ . All modes decay at the uncoupled damping rate of -1 yr^{-1} before merging. After merging, the coupled Rossby and Kelvin modes become destabilized, whereas the slow modes decay more rapidly with increasing σ .

With increasing magnitude for η the coupled Rossby and westward slow modes merge. For $|\eta|$ smaller than this merging value, the frequency of the coupled Rossby (westward slow) mode decreases (increases)

with increasing $|\eta|$. After merging, the frequency of the coupled Rossby mode is identical with that of the westward slow mode and decreases with increasing $|\eta|$ until reaching the bounded eigenfunction constraint. In contrast, the coupled Kelvin mode does not merge with the eastward slow mode throughout the range shown. The frequency of the coupled Kelvin mode (eastward slow mode) decreases (increases) with increasing $|\eta|$. As $|\eta|$ increases, the coupled Rossby mode becomes unstable, whereas all other modes are damped. Neither the frequency nor growth rate of the eastward slow mode is sensitive to η .

The effects of μ , σ , and η on the coupled mode's frequency and stability are largely dependent upon the zonal phase lag θ between the wind stress and SST anomalies. With $\theta = 0.1\pi$ (not shown), the coupled Rossby and Kelvin modes do not merge with the slow modes, and it is the slow modes that become unstable with increasing these parameters while the coupled Rossby and Kelvin modes decay. Growth or decay of the coupled modes, which is determined by the correlation between the lagged SST (wind) and the ocean currents, is very sensitive to θ .

2) KELVIN WAVE SPEED c

The effects of c on the frequency and stability of the coupled modes using the model parameters of Table 1 are shown in Fig. 13. The frequency of the coupled

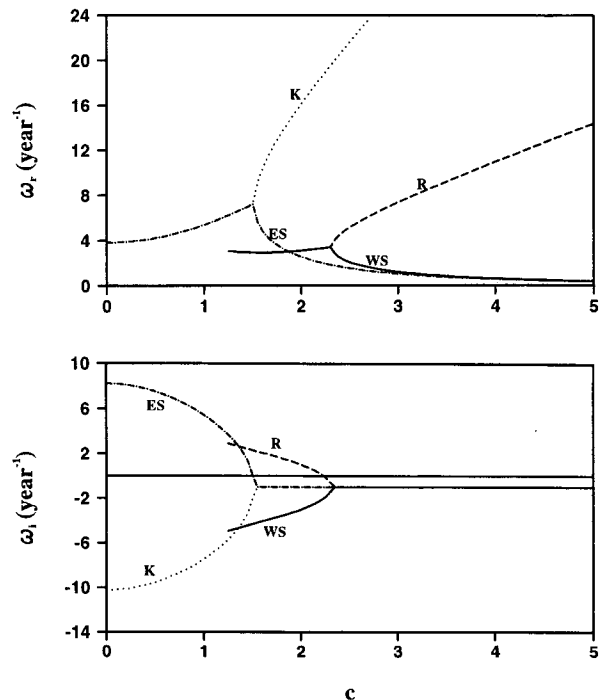


FIG. 13. As in Fig. 10 but as a function of oceanic Kelvin wave speed c (m s^{-1}) with $k = \pm 3.0 \times 10^{-7} \text{ m}^{-1}$.

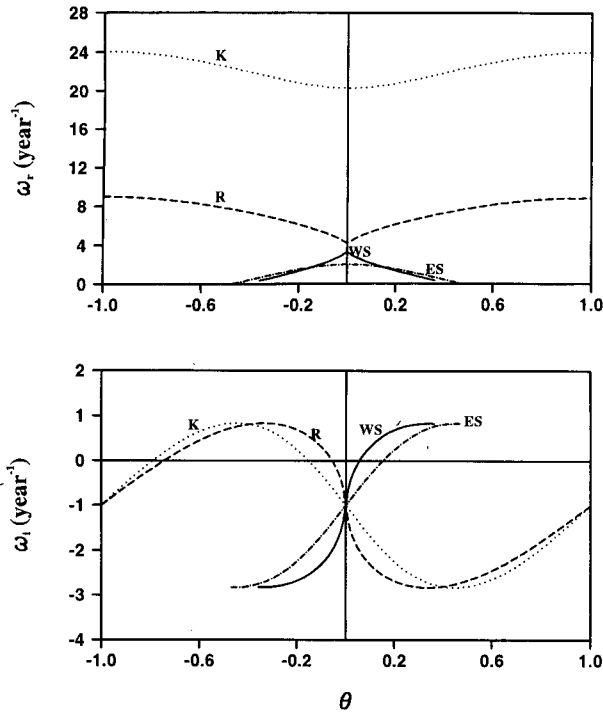


FIG. 14. As in Fig. 10 but as a function of zonal phase difference θ (π) between the zonal wind stress and SST anomalies with $k = \pm 3.6 \times 10^{-7} \text{ m}^{-1}$.

3) ZONAL PHASE DIFFERENCE θ

The effects of θ on the frequency and stability of the coupled modes using the model parameters of Table 1 are shown in Fig. 14. The frequency of all modes is symmetric about $\theta = 0$. For the slow modes, frequency decreases with increasing $|\theta|$, and bounded solutions do not exist when $|\theta|$ exceeds a parameter-dependent value. Large zonal phase differences, therefore, do not favor slow modes. On the other hand, the coupled Rossby and Kelvin mode frequencies increase slowly with increasing $|\theta|$. The growth rate of all modes is antisymmetric about $\theta = 0$ relative to the uncoupled damping rate of -1 yr^{-1} . The growth rate of the slow modes increases with increasing θ , and θ must be positive for instability. Conversely, the coupled Rossby and Kelvin modes require negative θ for instability. The magnitude and sign of θ , therefore, play important roles in the instability properties of these coupled equatorial modes. Both models (e.g., Gill 1980) and observations (e.g., Rasmusson et al. 1983) suggest that θ between 0.1π and 0.2π provides the best representative values.

4) THE PARAMETERS γ AND α

The Rayleigh friction/Newtonian cooling coefficient γ and the thermal damping coefficient α set the mechanical and thermal dissipation rate for the wave

Rossby and Kelvin modes decreases with decreasing c , and conversely for the westward and eastward slow modes prior to their merging. After merging, the westward and eastward slow modes share the same frequency with the coupled Rossby and Kelvin modes, respectively. Before merging all modes decay at the uncoupled damping rate of -1 yr^{-1} . After merging, the coupled Rossby and the eastward slow modes become unstable, while the coupled Kelvin and westward slow modes become increasingly more damped with decreasing c .

The results for the eastward slow mode are consistent with the numerical findings of Wang and Weisberg (1994a). The explanation follows from the change in the background state buoyancy as specified by c . Decreasing c , by decreasing buoyancy, increases the divergence for a given value of surface current since the ratio of thermocline thickness perturbation to current perturbation is $h/u = H_0/c$. Increasing the oceanic divergence increases the eastward slow mode growth rate. It is noted that the physics of varying c is quite different from that of varying the time derivatives of the oceanic dynamical equations as suggested by Neelin (1991). Varying the time derivatives of the oceanic dynamical equations distorts the effects of wave speed independent of buoyancy, whereas the importance of c herein is its effect on buoyancy.

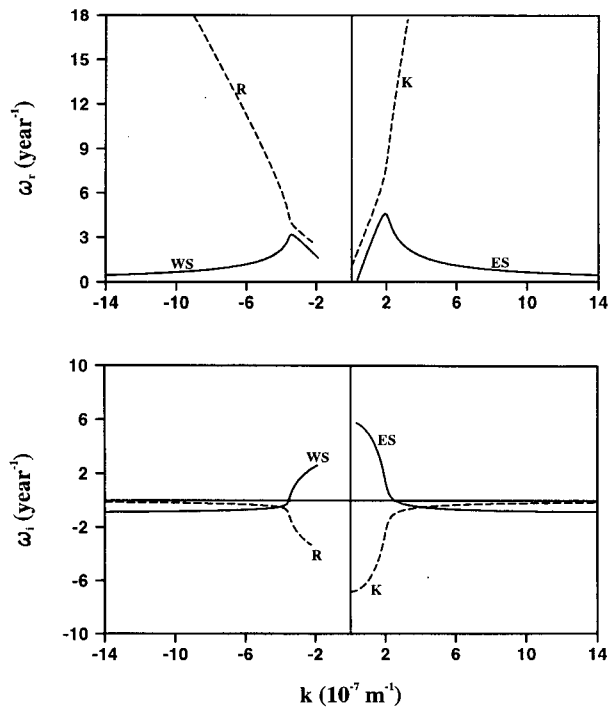


FIG. 15. As in Fig. 2 except Rayleigh friction/Newtonian cooling coefficient $\gamma = 0$.

modes, respectively. While not shown, these sensitivities were also examined. The frequency of the coupled Rossby and Kelvin (westward and eastward slow) modes increases (decreases) slowly with increasing γ , whereas the frequency of the coupled Rossby (westward slow) mode decreases (increases) with increasing α , while the frequency of coupled Kelvin and eastward slow modes is not sensitive to α . Interestingly, the growth rate of the eastward slow mode slowly increases with γ and, as can be seen by performing the fast-wave limit, this is due to zonal SST advection.

In order to further illustrate the roles of γ and α in the coupled modes, the frequency and growth rate are shown as a function of k in Figs. 15 and 16 for $\gamma = 0$ and $\alpha = 0$, respectively, using $\theta = 0.1\pi$ and the model parameters of Table 1. Compared with Fig. 2, Fig. 15 shows that the growth rates of the slow modes are relatively unaffected at all wavenumbers, whereas the decay rates of the coupled Rossby and Kelvin modes are smaller. On the other hand, Fig. 16 shows that the growth rates of the coupled Rossby and Kelvin modes are relatively unaffected at all wavenumbers, whereas the slow modes no longer decay. Thus, the effect of Rayleigh friction/Newtonian cooling (thermal damping) is mainly to damp the coupled Rossby and Kelvin modes (the slow modes) since the coupled Rossby and Kelvin modes (the slow modes) originate from the dynamical (thermodynamical) equation in which γ (α) enters the coupled system. It follows that damping for the coupled Rossby and Kelvin modes (the slow modes) is mainly mechanical (thermal).

5. Discussion and summary

A coupled ocean–atmosphere model, simplified for analytical tractability, is studied for insights on the stability properties of coupled equatorial modes. The paper extends the work of Wang and Weisberg (1994b) by relaxing the assumption of equal coefficients for Rayleigh friction/Newtonian cooling and thermal damping and by including a zonal phase difference between the anomalies of τ^x and SST. The two primary restrictive assumptions remaining are 1) the proportionality between the anomalies of τ^x and SST and 2) the spatial homogeneity in the thermodynamic parameters. The first of these is more restrictive than the Gill (1980) atmosphere used by Hirst (1986) and it may account for the differences obtained here with similar ocean thermodynamics.

Allowing a zonal phase difference between the τ^x and SST anomalies makes the first assumption more realistic. However, spatially uniform coupling remains erroneous. In nature, coupling varies both in space and time. For example, Wakata and Sarachik (1994) argued that coupling occurs differently during the warm and cold phases of ENSO, and numerous authors have argued that coupling is strongest over the eastern Pacific owing to the largest SST anomalies there. The

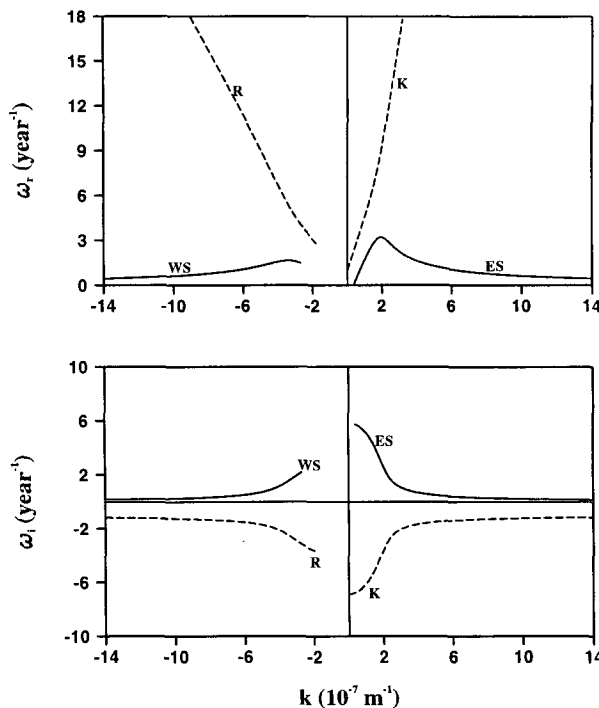


FIG. 16. As in Fig. 2 except thermal damping coefficient $\alpha = 0$.

second assumption of spatial homogeneity in thermodynamic parameters renders the SST equation overly simplistic since it does not allow spatial variations of background state processes, for example, the reason why the SST anomalies are largest over the eastern Pacific. Nevertheless, these simplifications provide an analytical basis for diagnosing instabilities that may have applicability to more realistic systems.

A property of the solutions is that the meridional scales for all coupled equatorial wave modes at low frequency are larger than those associated with an oceanic Rossby radius of deformation. A similar finding was discussed for neutral modes under a much more restrictive set of assumptions by Wang and Weisberg (1994b). This meridional scale increase appears in western Pacific observations (e.g., White et al. 1987, 1989; Kessler 1990), in GCM simulations of the coupled ocean–atmosphere system (e.g., Barnett et al. 1991; Chao and Philander 1993), and in simple numerical experiments using a Gill (1980) atmosphere (e.g., Hirst 1988; Wang and Weisberg 1994a). Using the high-resolution SST product of Reynolds and Smith (1995), this is also a property of eastern Pacific SST anomalies as shown in Fig. 17. So, while the assumed spatially uniform coupling may lead to an overestimate of the meridional length scale as frequency tends toward zero, this analytically obtained meridional scale increase does appear to be physically relevant. Additionally, the northeastward isoline tilt for unstable east-

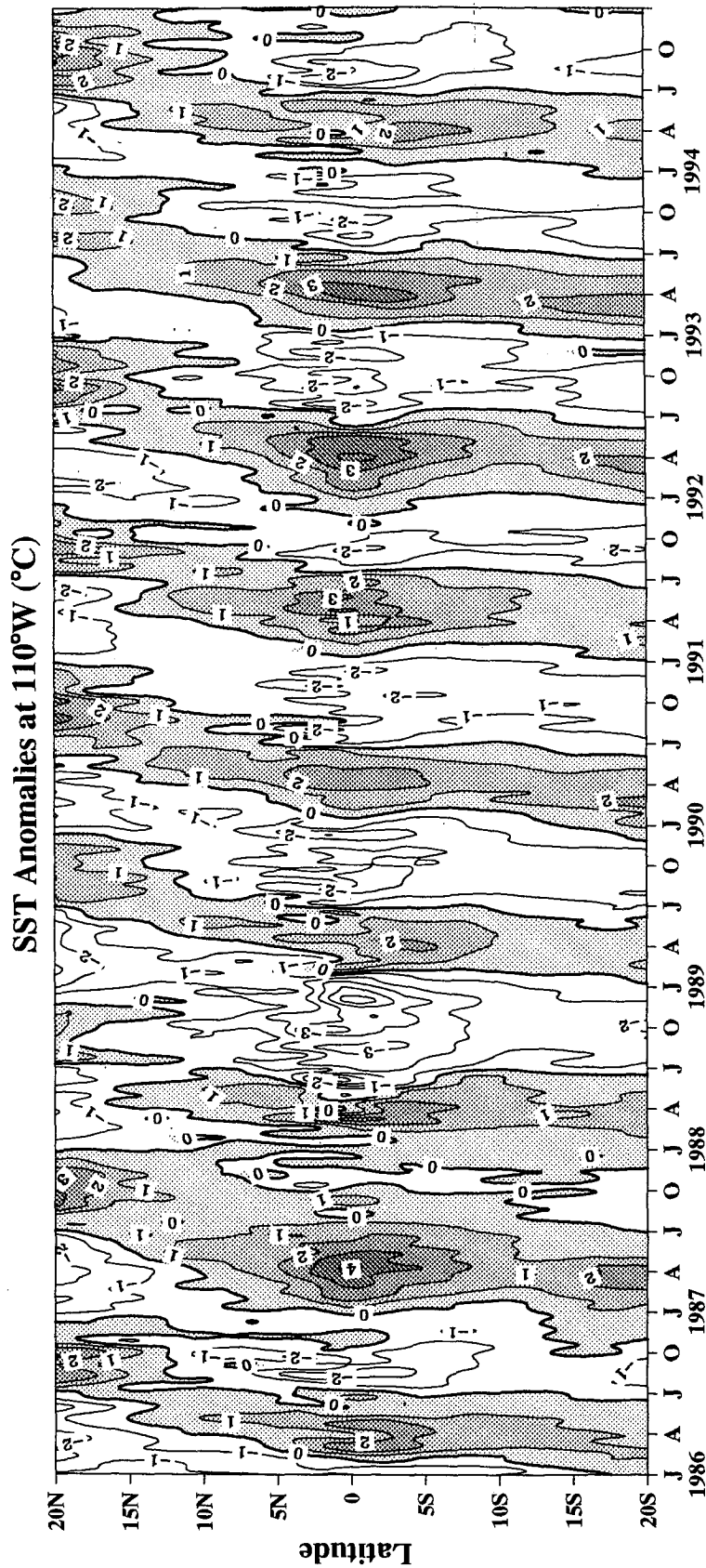


FIG. 17. SST anomalies as a function of latitude and time at 110°W calculated from the high-resolution SST product of Reynolds and Smith (1995). The anomalies are calculated by subtracting the 9-year mean SST from the total SST. The data have been low-pass filtered to remove oscillations at timescales shorter than one month. Shading denotes positive SST anomalies with a contour interval of 1°C. Note that the meridional scales of SST anomalies are much larger than the oceanic equatorial Rossby radius of deformation.

ward modes is consistent with observed SST patterns (e.g., Latif and Barnett 1995).

A simple physical basis exists for the meridional scale increase. For a system having separate atmosphere and ocean physics, there should exist two intrinsically different meridional scales with the atmosphere scale being larger than the ocean scale. Since the atmosphere and ocean are coupled, it follows that the scale of the coupled modes should take on an intermediate value. Under the present set of assumptions there is only one intrinsic scale—that of the ocean; however, a meridional scale broadening still occurs. An explanation follows from the coupling-induced wind stress curl in the vorticity equation. Without wind stress curl, conservation of absolute vorticity requires that the meridional component of velocity tends to zero at low frequency. This leaves the intrinsic β -plane radius of deformation determined by the oceanic buoyancy and the earth's rotation as the meridional scale. By including wind stress curl as an external torque, absolute vorticity is not conserved and the meridional component of velocity then tends toward a slowly varying Sverdrup balance. The meridional scale is then determined by the oceanic buoyancy and the earth's rotation as well as air–sea coupling. Physically, it is the wind stress curl that broadens the meridional scale by altering the slope of the thermocline. This may be shown mathematically by substituting the solutions into the vorticity equation demonstrating how the dispersion relationship is modified. As the simplest case, the eigenfunctions of Eqs. (3.24–26) for eastward propagating modes show that the meridional scale for these coupled modes is $L_c = (kc^2/\beta\omega_r)^{1/2} = L(c/c_c)^{1/2}$, where $L = (c/\beta)^{1/2}$ is the oceanic equatorial Rossby radius of deformation, c is the conventional Kelvin wave speed, and c_c is the modified phase speed of coupled equatorial modes. Since c_c is smaller than c , the meridional scale of the coupled modes L_c is larger than the oceanic equatorial radius of deformation L .

The growth, decay, and meridional phase gradient properties of the modes obtained herein, relative to the neutral modes of Wang and Weisberg (1994b), are a consequence of using different values for the dissipation constants and employing a zonal phase lag between the τ^x and SST anomalies. These solutions (albeit with an overly simplified atmosphere model) allow for the coexistence of westward and eastward slow modes along with the coupled Rossby and Kelvin modes. Of the four gravest modes, two can be destabilized by varying the model parameters, one propagating westward and another propagating eastward. If $\theta = 0$ and $\gamma = \alpha$, the coupled Rossby and Kelvin modes merge with the westward and eastward slow modes, respectively. When they merge, the coupled Rossby (Kelvin) and westward (eastward) slow modes split into two branches: one growing and the other decaying. However, for other parameter choices, the coupled Rossby and Kelvin modes remain distinct from the

slow modes. Thus, the coupled Rossby and Kelvin modes generally have different structure and phase speed than their slow mode counterparts. All unstable (stable) modes display a positive (negative) correlation between τ^x and the current, satisfying the necessary condition for instability.

Coupled mode stability is sensitive to the model parameters. For the zonal phase lag θ between the τ^x and SST anomalies the frequency for all modes is symmetric about $\theta = 0$, whereas the stability is antisymmetric about $\theta = 0$ relative to the uncoupled damping rate. Positive (negative) θ represents τ^x anomalies located to the west (east) of the SST anomalies. Therefore, coupled mode instability is determined by the relative position between τ^x and SST (e.g., Battisti et al. 1989). The slow modes and coupled Rossby or Kelvin modes can be destabilized if the τ^x anomaly is located to the west and east of the SST anomaly, respectively. The simplest atmospheric models [e.g., Gill (1980)] show the former, suggesting that unstable slow modes are favored by this coupled system. However, the relationship between SST, atmospheric heating, and resultant winds remains in question throughout the basin, and in the western Pacific the negative θ unstable Kelvin wave frequencies correspond to the frequencies of observed intraseasonal Kelvin waves (e.g., McPhaden and Taft 1988). The stability effects of the mechanical γ and thermal α damping parameters are also interesting. The coupled Rossby and Kelvin (slow) modes are mainly damped by γ (α) since the coupled Rossby and Kelvin (slow) modes originate from the time derivatives of the oceanic dynamical (thermodynamical) equation in which γ (α) enters the coupled system. Subtle effects, such as a growth rate increase for the eastward slow mode with increasing γ through the effect of zonal temperature advection, are also found. Given that $\omega = \omega(k, \mu, \sigma, \eta, c, \theta, \gamma, \alpha)$ even in this relatively simple model, the stability properties of coupled modes are very complicated. Generally, for this system, an increase in the coupling, warming, and zonal mean SST gradient coefficients and a decrease in the Kelvin wave speed will increase the growth rate of a particular unstable mode.

While substantial progress has been made over the past two decades in describing and understanding ENSO variability, neither observations nor numerical simulations of the coupled tropical ocean–atmosphere system have brought closure on the details of ENSO evolution. Here we have described the stability of equatorial modes within a model employing simplifying assumptions to achieve analytical tractability. Coupled Rossby and Kelvin modes were found to coexist with eastward and westward slow modes. These modes may merge in parameter space with instability favoring the slow modes, especially when τ^x anomalies are positioned west of SST anomalies. Coupling in this model profoundly affects the structure, propagation, and stability properties of equatorial modes at low frequency.

If this is true of nature, it follows that determining where within the equatorial waveguide and with what efficiency this coupling occurs (the two most limiting assumptions of this model) would be critical to more fully understand the coupled ocean–atmosphere interactions that constitute ENSO.

Acknowledgments. The comments by Drs. M. Cane, J. McCreary, D. Tang, S. Xie, and anonymous reviewers are appreciated. We would like to thank Dr. R. W. Reynolds at the National Centers for Environmental Prediction for providing the SST data. Support for this work was provided by the Division of Ocean Sciences, National Science Foundation, Grant OCE-9100024. The very positive influences of Dr. S. Hayes on collaborative ENSO studies are also acknowledged.

REFERENCES

- Anderson, D. L. T., and J. P. McCreary, 1985: Slowly propagating disturbances in a coupled ocean–atmosphere model. *J. Atmos. Sci.*, **42**, 615–629.
- Barnett, T. P., M. Latif, E. Kirk, and E. Roeckner, 1991: On ENSO physics. *J. Climate*, **4**, 487–515.
- , —, N. Graham, M. Flügel, S. Pazan, and W. White, 1993: ENSO and ENSO-related predictability. Part I: Prediction of equatorial Pacific sea surface temperature with a hybrid coupled ocean–atmosphere model. *J. Climate*, **6**, 1545–1566.
- Battisti, D. S., 1988: The dynamics and thermodynamics of a warming event in a coupled tropical atmosphere–ocean model. *J. Atmos. Sci.*, **45**, 2889–2919.
- , and A. C. Hirst, 1989: Interannual variability in the tropical atmosphere–ocean model: Influence of the basic state, ocean geometry, and nonlinearity. *J. Atmos. Sci.*, **45**, 1687–1712.
- , —, and E. S. Sarachik, 1989: Instability and predictability in coupled atmosphere–ocean models. *Philos. Trans. Roy. Soc. London A*, **329**, 237–247.
- Bjerknes, J., 1969: Atmospheric teleconnections from the equatorial Pacific. *Mon. Wea. Rev.*, **97**, 163–172.
- Cane, M. A., M. Munnich, and S. E. Zebiak, 1990: A study of self-excited oscillations of the tropical ocean–atmosphere system. Part I: Linear analysis. *J. Atmos. Sci.*, **47**, 1562–1577.
- Chao, Y., and S. G. H. Philander, 1993: On the structure of the Southern Oscillation. *J. Climate*, **6**, 450–469.
- Gill, A. E., 1980: Some simple solutions for heat-induced tropical circulation. *Quart. J. Roy. Meteor. Soc.*, **106**, 447–462.
- , 1985: Elements of coupled ocean–atmosphere models for the Tropics. *Coupled Ocean–Atmosphere Models*, Elsevier Oceanogr. Ser., Vol. 40, J. C. Nihoul, Ed., Elsevier, 303–327.
- Hirst, A. C., 1986: Unstable and damped equatorial modes in simple coupled ocean–atmosphere models. *J. Atmos. Sci.*, **43**, 606–630.
- , 1988: Slow instabilities in tropical ocean basin–global atmosphere models. *J. Atmos. Sci.*, **45**, 830–852.
- Jin, F. F., and J. D. Neelin, 1993a: Modes of interannual tropical ocean–atmosphere interaction—A unified view. Part I: Numerical results. *J. Atmos. Sci.*, **50**, 3477–3503.
- , and —, 1993b: Modes of interannual tropical ocean–atmosphere interaction—A unified view. Part III: Analytical results in fully coupled case. *J. Atmos. Sci.*, **50**, 3523–3540.
- Kessler, W. S., 1990: Observations of long Rossby waves in the northern tropical Pacific. *J. Geophys. Res.*, **95**, 5183–5219.
- Latif, M., and T. P. Barnett, 1995: Interactions of the tropical oceans. *J. Climate*, **8**, 952–964.
- Lau, K. M., 1981: Oscillation in a simple equatorial climate system. *J. Atmos. Sci.*, **38**, 248–261.
- Lindzen, R. S., and S. Nigam, 1987: On the role of sea surface temperature gradients in forcing low-level winds and convergence in the Tropics. *J. Atmos. Sci.*, **44**, 2418–2436.
- Matsuno, T., 1966: Quasi-geostrophic motions in the equatorial area. *J. Meteor. Soc. Japan*, **2**, 25–43.
- McCreary, J. P., 1983: A model of tropical ocean–atmosphere interaction. *Mon. Wea. Rev.*, **111**, 370–387.
- McPhaden, M. J., and B. A. Taft, 1988: On the dynamics of seasonal and intraseasonal variability in the eastern equatorial Pacific Ocean. *J. Phys. Oceanogr.*, **18**, 1713–1732.
- Neelin, J. D., 1991: The slow sea surface temperature mode and the fast-wave limit: Analytic theory for tropical interannual oscillations and experiments in a hybrid coupled models. *J. Atmos. Sci.*, **48**, 584–606.
- , and F. F. Jin, 1993: Modes of interannual tropical ocean–atmosphere interaction—A unified view. Part II: Analytical results in the weak-coupling limit. *J. Atmos. Sci.*, **50**, 3504–3522.
- Philander, S. G. H., T. Yamagata, and R. C. Pacanowski, 1984: Unstable air–sea interactions in the Tropics. *J. Atmos. Sci.*, **41**, 604–613.
- Rasmusson, E. M., P. A. Arkin, A. F. Krueger, R. S. Quiroy, and R. W. Reynolds, 1983: The equatorial Pacific atmospheric climate during 1982–83. *Trop. Ocean–Atmos. Newslett.*, **21**, 2–3.
- Rennick, M. A., 1983: A model of atmosphere–ocean coupling in El Niño. *Trop. Ocean–Atmos. Newslett.*, **15**, 2–4.
- Reynolds, R. W., and T. M. Smith, 1995: A high-resolution global sea surface temperature climatology. *J. Climate*, **8**, 1571–1583.
- Schopf, P. S., and M. J. Suarez, 1990: Ocean wave dynamics and timescale of ENSO. *J. Phys. Oceanogr.*, **20**, 629–645.
- Suarez, M. J., and P. S. Schopf, 1988: A delayed action oscillator for ENSO. *J. Atmos. Sci.*, **45**, 3283–3287.
- Wakata, Y., and E. S. Sarachik, 1991: Unstable coupled atmosphere–ocean basin modes in the presence of a spatially varying basic state. *J. Atmos. Sci.*, **48**, 2060–2077.
- , and —, 1994: Nonlinear effects in coupled atmosphere–ocean basin modes. *J. Atmos. Sci.*, **51**, 909–920.
- Wang, C., and R. H. Weisberg, 1994a: On the “slow mode” mechanism in ENSO-related coupled ocean–atmosphere models. *J. Climate*, **7**, 1657–1667.
- , and —, 1994b: Equatorially trapped waves of a coupled ocean–atmosphere system. *J. Phys. Oceanogr.*, **24**, 1978–1998.
- White, W. B., S. E. Pazan, and M. Inoue, 1987: Hindcast/forecast of ENSO events based on redistribution of observed and model heat content in the western tropical Pacific, 1964–1986. *J. Phys. Oceanogr.*, **17**, 264–280.
- , Y. H. He, and S. E. Pazan, 1989: Redistribution of subsurface thermal structure during the onset of the 1982–83 and 1986–87 ENSO events and the 1984–85 anti-ENSO event. *J. Phys. Oceanogr.*, **19**, 1397–1406.
- Yamagata, T., 1985: Stability of a simple air–sea coupled model in the Tropics. *Coupled Ocean–Atmosphere Models*, Elsevier Oceanogr. Ser., Vol. 40, J. C. Nihoul, Ed., Elsevier, 637–657.
- Zebiak, S. E., 1993: Air–sea interaction in the equatorial Atlantic region. *J. Climate*, **6**, 1567–1586.
- , and M. A. Cane, 1987: A model El Niño–Southern Oscillation. *Mon. Wea. Rev.*, **115**, 2262–2278.